Study of quantum decoherence at the Protvino to ORCA experiment

Chinmay Bera[*] and K. N. Deepthi[†]

Department of Physics, École Centrale School of Engineering, Mahindra University, Hyderabad, Telangana, 500043, India

(Received 8 May 2024; accepted 30 July 2024; published 29 August 2024)

Protvino to ORCA (oscillation research with cosmics in the abyss) (P2O) is an upcoming neutrino oscillation experiment with a very long baseline of 2595 km. Because of the substantial baseline, this experiment provides a unique opportunity to study the Earth matter effects over very large distances. This makes it a suitable experiment to investigate the environmental decoherence in neutrino oscillations, where the neutrino system could interact with a stochastic environment and lead to a loss in the coherence of neutrino states. In this work, we consider an open quantum system framework to simulate the neutrino oscillations in the P2O experiment and obtain bounds on the decoherence parameters in different phenomenological models. Here, we also consider that the decoherence parameter Γ depends on neutrino energy E_ν as $\Gamma_{jk}(E_\nu) = \Gamma_0(\frac{E_\nu}{E_0})^n$. Furthermore, assuming the presence of decoherence in nature, we study the effect of it on the determination of neutrino mass hierarchy and *CP* violation at the P2O experiment.

DOI: 10.1103/PhysRevD.110.035035

I. INTRODUCTION

Over the past few years, leading neutrino experiments have been diligently collecting data to estimate the neutrino oscillation parameters precisely. To date, the majority of the data from these experiments aligns with the conventional three-flavor neutrino oscillation framework, characterized by three mixing angles, two mass square differences, and a Dirac charge-parity (*CP*) phase. Nevertheless, the forthcoming high-precision neutrino oscillation experiments provide a significant opportunity to probe subleading new physics phenomenon. One such interesting phenomenon is the environmentally induced decoherence among the neutrino states passing through the Earth matter.

The standard three-flavor neutrino oscillation phenomenology considers neutrinos to be isolated from the environment, and the coherence of the neutrino states is preserved over very long distances. However, several theories [1–5] propose the possibility of interaction of neutrinos with a stochastic environment, leading to the loss of coherence in the neutrino states. This phenomenon is called quantum neutrino decoherence [6–28], and it is different in its origin from the quantum mechanical wave packet decoherence [29–33]. In this paper, we consider only the former case.

In recent years, significant research efforts have been carried out in constraining the decoherence parameters. In Ref. [34], the authors have analyzed Super-Kamiokande atmospheric neutrino experiment data and obtained bounds on the decoherence parameter $\Gamma < 3.5 \times 10^{-23}$ GeV (90% CL). In Ref. [35], the bounds on the decoherence parameters were obtained using main injector neutrino oscillation search (MINOS) data, while in Ref. [36], data from MINOS and Tokai to Kamioka (T2K) experiments have been analyzed to update the bounds on the decoherence parameter by assuming power-law dependency on the neutrino energy. The bounds obtained from the analysis of solar and Kamioka Liquid Scintillator Antineutrino Detector (KamLAND) data have been presented in Ref. [37]. In a further analysis, in Ref. [38], the authors included the recent KamLAND data. In a seminal paper (Ref. [39]), the authors pointed out that the 2σ tension between the T2K and NuMI Off-Axis ν_e Appearance (NOνA) data could be elevated by considering environmental decoherence of strength $\Gamma = (2.3 \pm 1.1) \times 10^{-23}$ GeV. The authors of Ref. [40] have analyzed the IceCube and DeepCore data on atmospheric neutrinos and reported the bounds on the Γ considering $n = 0, \pm 1, \pm 2$. Recently, in Ref. [41], the IceCube Collaboration reported bounds on Γ with atmospheric neutrinos for $n = 0$, 1, 2, 3. References [42,43] present the sensitivity studies of the Deep Underground Neutrino Experiment (DUNE) to the decoherence parameters. The authors in Ref. [44] have updated the limits on Γ by analyzing reactor data from

[*]Contact author: chinmay20pphy014@mahindrauniversity.edu.in

[†]Contact author: nagadeepthi.kuchibhatla@mahindrauniversity.edu.in

KamLAND, Daya Bay, and Reactor Experiment for Neutrino Oscillation (RENO) and accelerator data from T2K, NOνA, MINOS, and MINOS+. Additionally, they have simulated the upcoming Jiangmen Underground Neutrino Observatory (JUNO) and DUNE facilities to study their sensitivity to Γ. In a more recent study [45], the authors have obtained the sensitivity of the future long baseline The European Spallation Source neutrino super-beam (ESSnuSB) experiment to bound the decoherence parameter Γ and further investigated the *CPV* sensitivity of the experiment in the presence of decoherence.

In an open quantum system framework, the neutrino system interacts with the environment, leading to the loss of quantum coherence among the neutrino states. This decoherence effect manifests as a damping term $e^{-\Gamma L}$ in the neutrino oscillation probabilities, where Γ is the decoherence parameter and L is the distance traveled by the neutrinos. Γ can be parametrized using power-law dependency, i.e., $\Gamma \propto E_\nu^n$, where E_ν is the neutrino energy and the value of n depends on the origin of the decoherence model. In this context, without delving into the origin of the decoherence effect, we perform a phenomenological study of the effect of quantum neutrino decoherence in the Protvino to ORCA (P2O) experiment. P2O is an upcoming neutrino oscillation experiment with a substantial baseline of 2595 km [46,47]. This very large baseline of the P2O experiment makes it an ideal candidate to study the impact of environmentally induced decoherence on the neutrino oscillations.

This paper is structured as follows. In Sec. II, we present a concise overview of the density matrix formalism which is employed to derive the neutrino oscillation probabilities. We discuss the experimental and simulation details of our analysis in Sec. III. In Sec. IV, we examine the impact of environmental decoherence on various oscillation channels (baseline 2595 km), taking into account the power-law dependencies of decoherence on neutrino energy. In addition, we study the consequences of assuming the presence of decoherence in the true spectrum and assess the significance of P2O to determine the mass hierarchy and *CP* violation. Finally, we conclude our results in Sec. V.

II. THEORETICAL FORMULATION

In an open quantum system framework, the neutrino subsystem can interact very weakly with the stochastic environment. Keeping a phenomenological approach, we discuss the dissipative effects of the decoherence on neutrino oscillations in a model-independent way. To achieve this, we consider density matrix formalism and represent the time evolution of the density matrix using the Lindblad master equation [48,49]

$$\frac{d\rho_m(t)}{dt} = -i[H, \rho_m(t)] + \mathcal{D}[\rho_m(t)], \tag{2.1}$$

where ρ_m is the density matrix of neutrino in the mass basis and H is the Hamiltonian of the neutrino system. The decoherence effect is introduced through a dissipative term $\mathcal{D}[\rho_m(t)]$. Parametrization of the decoherence matrix is performed by imposing mathematical properties of the density matrix such as complete positivity and preserving trace normalization (probability must be positive and conserved with respect to time). Imposing complete positivity gives the Lindblad form of the dissipator as [50]

$$\mathcal{D}[\rho_m(t)] = \frac{1}{2}\sum_{n=1}^{N^2-1}\{[\mathcal{V}_n, \rho_m \mathcal{V}_n^\dagger] + [\mathcal{V}_n \rho_m, \mathcal{V}_n^\dagger]\}, \tag{2.2}$$

where N is the dimension of the Hilbert space and $\mathcal{V}_n$ are the operators arising from the interaction of the subsystem with the environment. In addition, we impose an increase in von Neumann entropy $S = -\mathrm{Tr}(\rho_m \ln \rho_m)$ [51,52] and conservation of average energy $\mathrm{Tr}(\rho_m H)$ of the neutrino system. These conditions lead to $\mathcal{V}_n = \mathcal{V}_n^\dagger$ and $[\mathcal{V}_n, H] = 0$ and imply that $\mathcal{V}_n$ and H are simultaneously diagonalizable. For a three-flavor neutrino system ($N = 3$), operators $\mathcal{V}_n$ ($n = 1, 2, \ldots, 8$) are the linear combinations of the Gell-Mann matrices. Substituting for $\mathcal{V}_n$ in Eq. (2.2) and using the above-mentioned conditions simplifies the dissipator term to

$$\mathcal{D}[\rho_m(t)] = \begin{pmatrix} 0 & -\Gamma_{21}\rho_{12}(t) & -\Gamma_{31}\rho_{13}(t) \\ -\Gamma_{21}\rho_{21}(t) & 0 & -\Gamma_{32}\rho_{23}(t) \\ -\Gamma_{31}\rho_{31}(t) & -\Gamma_{32}\rho_{32}(t) & 0 \end{pmatrix}, \tag{2.3}$$

with

$$\Gamma_{jk} = \Gamma_{kj} = \frac{1}{2}\sum_{n=1}^{8}(d_{n,j} - d_{n,k})^2, \tag{2.4}$$

where $d_{n,j}$ and $d_{n,k}$ are the diagonal elements of $\mathcal{V}_n$ operator and j and k take the values 1,2,3.

Considering vacuum Hamiltonian in the mass basis $H = \mathrm{diag}(0, \Delta_{21}, \Delta_{31})$, where $\Delta_{jk} = \Delta m^2_{jk}/2E$, Δm^2_{jk} being the neutrino mass-square differences ($m_j^2 - m_k^2$), one can obtain $[H, \rho_m(t)]$ to be

$$[H, \rho_m(t)] = \begin{pmatrix} 0 & -\rho_{12}(t)\Delta_{21} & -\rho_{13}(t)\Delta_{31} \\ \rho_{21}(t)\Delta_{21} & 0 & -\rho_{23}(t)\Delta_{32} \\ \rho_{31}(t)\Delta_{31} & \rho_{32}(t)\Delta_{32} & 0 \end{pmatrix}. \tag{2.5}$$

The density matrix (mass basis) at time t is obtained by substituting Eqs. (2.3) and (2.5) in Eq. (2.1) as (see Ref. [21] and the appendix in Ref. [43] for a comprehensive overview)

$$\rho_m(t) = \begin{pmatrix} \rho_{11}(0) & \rho_{12}(0)\exp-(\Gamma_{21}+i\Delta_{21})^* t & \rho_{13}(0)\exp-(\Gamma_{31}+i\Delta_{31})^* t \\ \rho_{21}(0)\exp-(\Gamma_{21}+i\Delta_{21})t & \rho_{22}(0) & \rho_{23}(0)\exp-(\Gamma_{32}+i\Delta_{32})^* t \\ \rho_{31}(0)\exp-(\Gamma_{31}+i\Delta_{31})t & \rho_{32}(0)\exp-(\Gamma_{32}+i\Delta_{32})t & \rho_{33}(0) \end{pmatrix}. \tag{2.6}$$

Equation (2.6) can be converted into the flavor basis using the modified Pontecorvo-Maki-Nakagawa-Sakata (PMNS) mixing matrix $\tilde{U}$, as we include the Mikheyev-Smirnov-Wolfenstein (MSW) effect. We consider the modified-mixing matrix ($\tilde{U}$) up to the first-order approximation, from Ref. [53], as

$$\tilde{\rho}_\alpha = \tilde{U}\tilde{\rho}_m\tilde{U}^\dagger. \tag{2.7}$$

The neutrino transition probability from initial flavor "ν_α" to final flavor "ν_β" in terms of density matrix is

$$P_{\alpha\beta}(t) = \mathrm{Tr}[\tilde{\rho}_\alpha(t)\tilde{\rho}_\beta(0)]. \tag{2.8}$$

The explicit form of the transition probability assuming ultrarelativistic neutrinos ($t \approx L$) is given by [40,43]

$$P_{\alpha\beta}(L) = \delta_{\alpha\beta} - 2\sum_{j>k}\mathrm{Re}(\tilde{U}_{\beta j}\tilde{U}^*_{\alpha j}\tilde{U}_{\alpha k}\tilde{U}^*_{\beta k}) + 2\sum_{j>k}\mathrm{Re}(\tilde{U}_{\beta j}\tilde{U}^*_{\alpha j}\tilde{U}_{\alpha k}\tilde{U}^*_{\beta k})\exp(-\Gamma_{jk}L)\cos\left(\frac{\tilde{\Delta}m^2_{jk}}{2E}L\right)$$
$$+ 2\sum_{j>k}\mathrm{Im}(\tilde{U}_{\beta j}\tilde{U}^*_{\alpha j}\tilde{U}_{\alpha k}\tilde{U}^*_{\beta k})\exp(-\Gamma_{jk}L)\sin\left(\frac{\tilde{\Delta}m^2_{jk}}{2E}L\right). \tag{2.9}$$

Note that in the absence of the decoherence effect, i.e., $\Gamma_{jk} = 0$, the probability expression reduces to the standard oscillation probability.

Let us examine Eq. (2.9) for the case of ν_e appearance probability term by term. For the case of $\alpha = \mu$, $\beta = e$, the nonzero terms of Eq. (2.9) take the form

$$\mathrm{I} = -2\sum_{j>k}\mathrm{Re}(\tilde{U}_{ej}\tilde{U}^*_{\mu j}\tilde{U}_{\mu k}\tilde{U}^*_{ek}), \tag{2.10}$$

$$\mathrm{II} = 2\sum_{j>k}\mathrm{Re}(\tilde{U}_{ej}\tilde{U}^*_{\mu j}\tilde{U}_{\mu k}\tilde{U}^*_{ek})\exp(-\Gamma_{jk}L)\cos\left(\frac{\tilde{\Delta}m^2_{jk}}{2E}L\right), \tag{2.11}$$

$$\mathrm{III} = 2\sum_{j>k}\mathrm{Im}(\tilde{U}_{ej}\tilde{U}^*_{\mu j}\tilde{U}_{\mu k}\tilde{U}^*_{ek})\exp(-\Gamma_{jk}L)\sin\left(\frac{\tilde{\Delta}m^2_{jk}}{2E}L\right). \tag{2.12}$$

(i) Term I is not affected by the decoherence parameter Γ_{jk}. When $j = 3$, $k = 2$, this term presents a resonance in the appearance probability at energy $E_\nu \sim 10$ GeV.

(ii) In term II [Eq. (2.11)] and term III [Eq. (2.12)], Γ_{jk} appear in the dissipative form $\sim\exp(-\Gamma_{jk}L)$, where L is the distance traveled by the neutrino beam and Γ_{jk} are the decoherence parameters that quantify the strength of the decoherence. Here, the coherence length can be obtained by $L_{\mathrm{coh}} = \frac{1}{\Gamma_{jk}}$.

(iii) In the absence of the damping term $\exp(-\Gamma_{32}L)$, terms II and III together cause a depression or dip in the probability and, in turn, cancel the resonance posed by term I. However, in the presence of decoherence, this dip disappears, and we see the resonance around $E \sim 10$ GeV in the appearance probability. A detailed analysis regarding this interplay between terms I, II, and III can be found in Ref. [43].

(iv) To illustrate the above-mentioned details regarding ν_e appearance probability, we plot term I, term (II + III) (without decoherence), and term (II + III) (with decoherence) for all values of j, $k = 1, 2, 3$, where $j > k$, in Fig. 1.

(v) We obtain three sets of $jk = 32, 31, 21$. In the left, middle, and right plots in Fig. 1, we have shown the effect of $\exp(-\Gamma_{32}L)$, $\exp(-\Gamma_{31}L)$, and $\exp(-\Gamma_{21}L)$, respectively. In each plot, we have presented three curves: blue (dot-dashed), green (dashed), and magenta (dotted), corresponding to term I, term (II + III) (without decoherence), and term (II + III) (with decoherence), respectively.

(vi) In the left plot (where $jk = 32$), we observe that, in the absence of decoherence, term I (bump) and term (II + III) (dip) cancel each other. However, in the presence of decoherence, the dip in term (II + III) gets removed and the bump in term I causes a peak in the probability around $E \sim 10$ GeV.

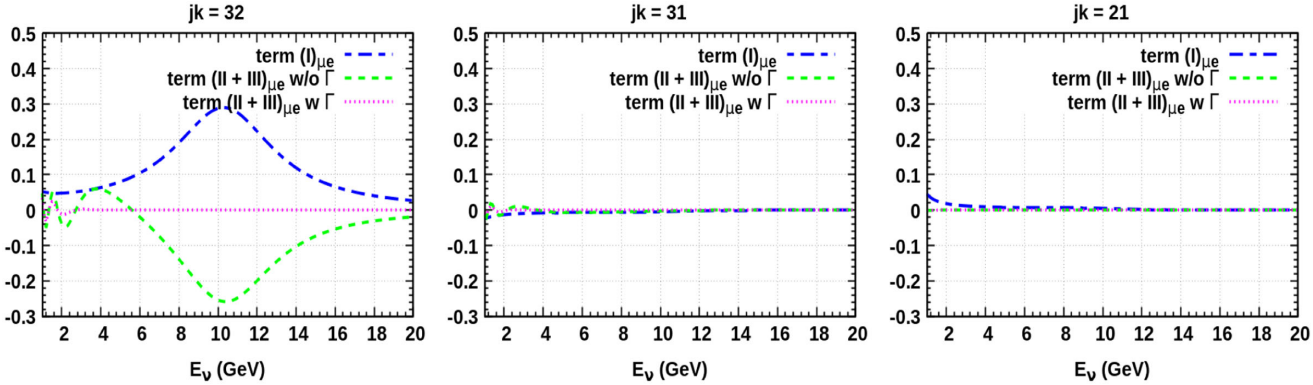

FIG. 1. Illustrative plots for the elements term I, term II + III (without decoherence), and term II + III (with decoherence) as a function of E_ν. The left, middle, and right plots correspond to $jk = 32$, 31, and 21, respectively.

(vii) However, in the case of the middle and right figures where the terms corresponding to $j = 3$, $k = 1$ and $j = 2$, $k = 1$ are plotted, we do not see any resonance or dip in the terms around $E \sim 10$ GeV.

(viii) This explains why when a model assumes $\Gamma_{32} = 0$ (for instance, in case II, where $\Gamma_{21} = \Gamma_{31}$, $\Gamma_{32} = 0$) the appearance probability does not get impacted by the presence of decoherence.

We consider a general power-law dependency of Γ_{jk} on the neutrino energy given by

$$\Gamma_{jk}(E_\nu) = \Gamma_0 \left(\frac{E_\nu}{E_0}\right)^n, \tag{2.13}$$

where Γ_0 is constant, E_0 is the reference energy taken as 1 GeV, and $n = 0, \pm 1, \pm 2$. Different physical origins explain the decoherence phenomena leading to different integral power-law dependencies [44].

From Eq. (2.4), it is clear that the Γ_{jk}'s are not independent of each other. In our analysis, we consider the cases mentioned in Table I, where at least two Γ_{jk}'s are activated simultaneously. Each case has a unique decoherence matrix [Eq. (2.3)] and, thus, damps different neutrino oscillation channels differently. In this work, we study the effect of the different power-law dependencies given in Eq. (2.13), for each of the cases in Table I.

TABLE I. The decoherence models considered in this work.

Cases	Assumptions on Γ_{jk}
Case I	$\Gamma_{21} = \Gamma_{31} = \Gamma_{32} \neq 0$
Case II	$\Gamma_{21} = \Gamma_{31}, \Gamma_{32} = 0$
Case III	$\Gamma_{21} = \Gamma_{32}, \Gamma_{31} = 0$
Case IV	$\Gamma_{31} = \Gamma_{32}, \Gamma_{21} = 0$

III. EXPERIMENTAL AND SIMULATION DETAILS

P2O is an upcoming long baseline neutrino oscillation experiment. The neutrino beam travels for about 2595 km from the Protvino accelerator complex before it reaches the 8 MT water cherenkov KM3NeT/ORCA detector. The initial plan is to have a 90 kW proton beam resulting in 0.8×10^{20} protons on target (POT) per year. A later upgrade of the beam facility targets a 450 kW proton beam. The resultant muon neutrino beam of 2–7 GeV passes through the upper mantle of Earth with matter density ~ 3.3 gm/cm^3 before it reaches the far detector that is currently being constructed in the Mediterranean Sea. The oscillation channels of utmost interest are $\nu_\mu \to \nu_e$, $\nu_\mu \to \nu_\mu$ channels and the corresponding antineutrino channels.

We assumed a total exposure of 6 yr, where 3 yr run-time is for the neutrino beam and 3 yr for the antineutrino beam. In the standard three-flavor oscillation scenario, the simulated data from 3 yr of neutrino mode (assuming a 90 kW beam) resulted in a total of $\sim 4800 \nu_\mu$ disappearance events and $\sim 2600 \nu_e$ appearance events at the far detector. On the other hand, in the antineutrino mode, we found ~ 1406 disappearance events and ~ 80 appearance events assuming normal ordering, $\theta_{23} = 45°$, and $\delta_{CP} = 270°$. The fraction of events classified as tracks (muon) and showers (electron) are taken from Fig. 99 in Ref. [47]. The energy resolution of the detector is considered $\approx 30\%$ as given in Ref. [46]. Under the systematic uncertainties, we considered 5% on the signal normalization, 12% on the background normalization, and an 11% tilt error on both signal and background.

We have used the GLoBES software [54,55] to simulate the P2O experiment and perform our analysis. Considering the standard three-flavor oscillation picture, we reproduced the event spectra with respect to the true neutrino energy that is reported in Ref. [46]. In this work, we simulated the data corresponding to 90 kW proton beam

TABLE II. True oscillation parameters and 3σ ranges have been considered in our analysis are taken from NuFIT [58].

Parameters	True values	3σ ranges
$\sin^2\theta_{12}$	0.304	Fixed
$\sin^2\theta_{13}$	0.0222	Fixed
$\sin^2\theta_{23}$	0.573	[0.405 : 0.620]
δ_{CP}	194°	[0 : 360°]
$\frac{\Delta m^2_{21}}{10^{-5}\ \mathrm{eV}^2}$	7.42	Fixed
$\frac{\Delta m^2_{31}}{10^{-3}\ \mathrm{eV}^2}$ (NH)	2.515	[2.431 : 2.599]
$\frac{\Delta m^2_{31}}{10^{-3}\ \mathrm{eV}^2}$ (IH)	−2.498	[−2.584 : − 2.413]

resulting in 0.8×10^{20} POT per year and also 450 kW beam corresponding to the 4.0×10^{20} POT per year and total runtime 6 yr (3 yr for ν and 3 yr for $\bar{\nu}$ mode) in each case. Later, we incorporated a new oscillation probability engine into GLoBES by taking into account the effect of decoherence on neutrino propagation. The best-fit values of the standard oscillation parameters and their 3σ ranges used in the analysis are given in Table II. For the statistical analysis, the χ^2 function is calculated using Poisson chi-square function given by

$$\chi^2 = \min_{\alpha_s,\alpha_b} \sum_{\text{channels}} 2\sum_i \left[N_i^{\text{test}} - N_i^{\text{true}} + N_i^{\text{true}} \log\left(\frac{N_i^{\text{true}}}{N_i^{\text{test}}}\right)\right] + \alpha_s^2 + \alpha_b^2, \tag{3.1}$$

where N_i^{test} and N_i^{true} are the number of test and true events (signal + background) in the ith bin, respectively. α_s and α_b are the signal and background normalization errors, respectively, treated using the *pull method* [56,57]. The analysis window of the neutrino energy is considered from 2 to 12 GeV. We marginalize over the δ_{CP}, θ_{23}, and Δm^2_{31} in their 3σ ranges without assuming any priors.

IV. RESULTS AND DISCUSSION

In this segment, we outline the findings of our analysis across four subsections, each focusing on the cases mentioned in Table I. The sensitivity studies have been performed for both 90 and 450 kW proton beams in all the subsections, and the corresponding bounds of Γ_{jk} have been reported in Tables III and IV, respectively. Henceforth, we will refer to the simulations with 90 kW proton beam as P2O and that with 450 kW beam as P2O-upgrade.

In each subsection, first we show the effect of nonzero decoherence on the three oscillation channels $\nu_\mu \to \nu_e$ (left), $\nu_\mu \to \nu_\mu$ (middle), and $\nu_\mu \to \nu_\tau$ (right) for P2O baseline. To achieve this, we have considered the true values of the standard oscillation parameters given in the second column in Table II allowing Normal Hierarchy (NH). However, for the sensitivity studies, we have taken into account only the relevant oscillation channels $\nu_\mu \to \nu_e$, $\nu_\mu \to \nu_\mu$, $\bar{\nu}_\mu \to \bar{\nu}_e$, and $\bar{\nu}_\mu \to \bar{\nu}_\mu$. Each figure contains the standard neutrino propagation in matter (SM) and the nonzero decoherence assuming energy dependency index in Eq. (2.13) as $n = -2, -1, 0, 1, 2$. In each plot, we show five curves where green, magenta, blue, dark green, and red lines represent $n = -2$, -1, 0, 1, and 2, respectively.

Second, to quantify the sensitivity of the P2O experiment to the decoherence parameter Γ_{jk}, we plot χ^2 as a function of Γ_{jk} (test). We simulate the data by taking $\Gamma_{jk} = 0$ (true) and the test spectrum by considering $\Gamma_{jk} \neq 0$. We calculate χ^2 as described in Sec. III and obtain

$$\Delta\chi^2_\Gamma = \chi^2(\Gamma(\text{true}) = 0, \Gamma(\text{test}) \neq 0), \tag{4.1}$$

after marginalizing over θ_{23}, δ_{CP}, and $(\Delta m^2_{31})_{NH}$ in the test spectrum. Furthermore, we provide the expected bounds on Γ_{jk} obtained for P2O and P2O-upgrade in Tables III and IV, respectively.

Later, assuming the presence of decoherence in the true spectrum, we study the effect of nonzero Γ_{jk} on the

TABLE III. Bounds obtained in different cases for 90 kW beam power.

		Case I	Case II	Case III	Case IV
n	CL	$\Gamma_{21} = \Gamma_{31} = \Gamma_{32}$	$\Gamma_{21} = \Gamma_{31}$	$\Gamma_{21} = \Gamma_{32}$	$\Gamma_{31} = \Gamma_{32}$
$n = -2$	90%	8.06×10^{-23}	6.0×10^{-23}	1.008×10^{-22}	8.0×10^{-23}
	3σ	1.15×10^{-22}	1.11×10^{-22}	1.56×10^{-22}	1.15×10^{-22}
$n = -1$	90%	1.8×10^{-23}	1.36×10^{-23}	2.19×10^{-23}	1.75×10^{-23}
	3σ	2.55×10^{-23}	2.46×10^{-23}	3.37×10^{-23}	2.53×10^{-23}
$n = 0$	90%	3.76×10^{-24}	2.76×10^{-24}	4.26×10^{-24}	3.76×10^{-24}
	3σ	5.3×10^{-24}	5.18×10^{-24}	6.7×10^{-24}	5.23×10^{-24}
$n = 1$	90%	7.4×10^{-25}	5.4×10^{-25}	7.31×10^{-25}	7.3×10^{-25}
	3σ	1.04×10^{-24}	1.02×10^{-24}	1.23×10^{-24}	1.008×10^{-24}
$n = 2$	90%	1.24×10^{-25}	9.07×10^{-26}	1.007×10^{-25}	1.2×10^{-25}
	3σ	1.79×10^{-25}	1.87×10^{-25}	1.95×10^{-25}	1.74×10^{-25}

TABLE IV. Bounds obtained in different cases for 450 kW beam power.

		Case I	Case II	Case III	Case IV
n	CL	$\Gamma_{21}=\Gamma_{31}=\Gamma_{32}$	$\Gamma_{21}=\Gamma_{31}$	$\Gamma_{21}=\Gamma_{32}$	$\Gamma_{31}=\Gamma_{32}$
$n=-2$	90%	6.4×10^{-23}	3.9×10^{-23}	6.5×10^{-23}	6.4×10^{-23}
	3σ	9.0×10^{-23}	7.6×10^{-23}	1.1×10^{-22}	9.3×10^{-23}
$n=-1$	90%	1.4×10^{-23}	8.5×10^{-24}	1.5×10^{-23}	1.46×10^{-23}
	3σ	2.1×10^{-23}	1.75×10^{-23}	2.5×10^{-23}	2.0×10^{-23}
$n=0$	90%	3.1×10^{-24}	1.89×10^{-24}	2.5×10^{-24}	3.1×10^{-24}
	3σ	4.2×10^{-24}	4.0×10^{-24}	5.0×10^{-24}	4.7×10^{-24}
$n=1$	90%	6.2×10^{-25}	3.6×10^{-25}	4.2×10^{-25}	6.3×10^{-25}
	3σ	8.5×10^{-25}	7.7×10^{-25}	8.5×10^{-25}	8.1×10^{-25}
$n=2$	90%	7.8×10^{-26}	5.87×10^{-26}	6.0×10^{-26}	7.5×10^{-26}
	3σ	1.5×10^{-25}	1.4×10^{-25}	1.1×10^{-25}	1.3×10^{-25}

determination of mass hierarchy and the discovery *CP* violation at the P2O experiment. This study shows the consequence of not assuming decoherence in the theoretical hypothesis while it is present in nature. For this, we consider the 3σ value of Γ_{jk} obtained from Tables III and IV as the true values in each subsection.

The $\Delta\chi^2_{\rm MH}$ is defined as

$$\Delta\chi^2_{\rm MH}=\chi^2_{\rm true}(\Gamma\neq0,\Delta m^2_{31}>0)-\chi^2_{\rm test}(\Gamma=0,\Delta m^2_{31}<0). \tag{4.2}$$

Here, we marginalize over the test parameters θ_{23} and $\delta_{\rm CP}$.

The $\Delta\chi^2_{CPV}$ is given by

$$\begin{aligned}\Delta\chi^2_0&=\chi^2_{\rm true}(\delta_{CP}({\rm true}),\Gamma\neq0)-\chi^2_{\rm test}(\delta_{CP}=0,\Gamma=0),\\ \Delta\chi^2_\pi&=\chi^2_{\rm true}(\delta_{CP}({\rm true}),\Gamma\neq0)-\chi^2_{\rm test}(\delta_{CP}=\pi,\Gamma=0),\\ \Delta\chi^2_{CPV}&=\min[\Delta\chi^2_0,\Delta\chi^2_\pi].\end{aligned} \tag{4.3}$$

We marginalize over the test parameters θ_{23} and $(\Delta m^2_{31})_{\rm NH}$. The significance ($\sigma$) of P2O to discover the mass hierarchy (*MH*) and *CPV* is obtained by using $\sigma_{\rm MH/CPV}=\sqrt{\Delta\chi^2_{MH/CPV}}$.

A. Case I: $\Gamma_{21}=\Gamma_{31}=\Gamma_{32}\neq0$

In this case, we assume Γ_{21}, Γ_{31}, and Γ_{32} to be equal to 2.3×10^{-23} GeV and nonzero. Figure 2 shows the probability of the three oscillation channels $\nu_\mu\to\nu_e$, $\nu_\mu\to\nu_\mu$, and $\nu_\mu\to\nu_\tau$ in the left, middle, and right panels, respectively. Legends corresponding to each plot are mentioned in the figure. It can be seen that all three oscillation probabilities are significantly modified for the positive powers of $n\geq0$ when compared to the SM case (black curve). Additionally, in the left plot, when $n\geq0$, there is an extra peak around 10 GeV in the $P_{\mu e}$ channel. The probability $P_{\mu\mu}$ ($P_{\mu\tau}$) is higher (lower) than the SM probability in the energy window $E_\nu\sim4$–9 GeV and lower (higher) in the ranges $E_\nu\sim2$–4 GeV and $E_\nu>9$ GeV. The first oscillation peak (dip) in the ν_e appearance (ν_μ disappearance)

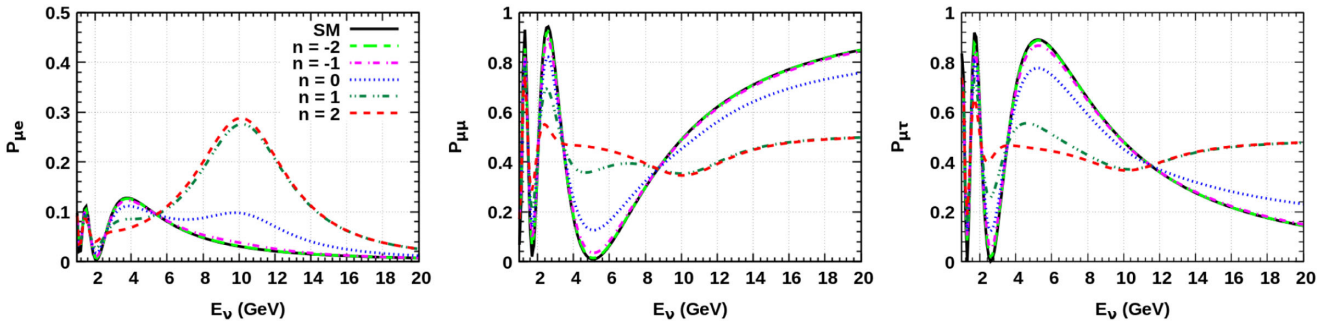

FIG. 2. Probability versus neutrino energy for ν_e appearance (left), ν_μ disappearance (middle), and ν_τ appearance (right) considering case I ($\Gamma_{21}=\Gamma_{31}=\Gamma_{32}=2.3\times10^{-23}$ GeV). The different colors correspond to the probabilities for the standard case, and various n dependencies are as mentioned in the legend.

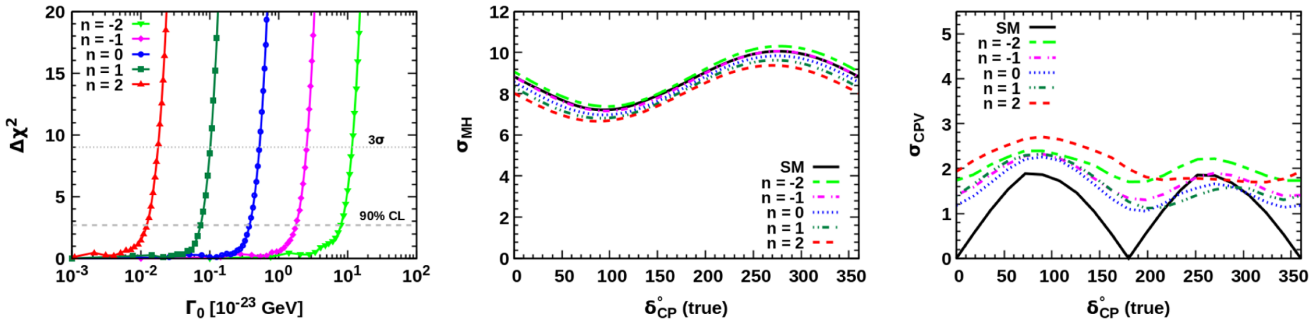

FIG. 3. Case I for the P2O experiment (90 kW beam). In the left, we present $\Delta\chi^2$ as a function of Γ_0 (test) based on power-law index $n = 0, \pm 1, \pm 2$. Horizontal dashed and dotted lines stand for 90% and 3σ CL, respectively. In the middle and right panels, we show the significance of the experiment to discover *MH* and *CP* violation.

channel is effected by the decoherence for the chosen set of decoherence parameters $\mathcal{O}(10^{-23}$ GeV). However, we noticed that this effect is not significant when the reference value of decoherence parameters is chosen to be $\mathcal{O}(10^{-24}$ GeV) and the extra peak around 10 GeV remains in place with lesser amplitude.

In the left plots in Figs. 3 and 4, we constrain Γ_{jk} presuming the conditions on decoherence parameters as given in case I. We calculate the test statistics using Eq. (4.1). The horizontal dashed and dotted lines correspond to 90% ($\sim 1.64\sigma$) and 3σ confidence level (CL), respectively. The corresponding bounds of these parameters for different n values are tabulated in the first column of Tables III and IV, respectively. From the leftmost plots in Figs. 3 and 4, it can be seen that the sensitivity to the decoherence parameter has slightly improved after the proton beam upgrade to 450 kW. It can be verified from the first column in Tables III and IV that the 3σ bounds on Γ_{jk} have improved by one order of magnitude for the cases with $n \geq 0$ for the P2O-upgrade (450 kW).

The $\Delta\chi^2_{MH}$ vs δ_{CP} (true) and $\Delta\chi^2_{CPV}$ vs δ_{CP} (true) are calculated at 3σ value of Γ_{jk} using Eqs. (4.2) and (4.3). The respective significances σ_{MH} (middle panel) and σ_{CPV} (right panel) are plotted for the standard case and for nonzero decoherence (with $n = 0, \pm 1, \pm 2$) in Figs. 3 and 4, respectively. For the 90 kW beam, we can see the *MH* sensitivity (middle plot) for $n = -2$ is higher than that for $n = 2$. The significance σ_{MH} is maximum around $\delta_{CP}(\text{true}) = 270°$. In the case of the 450 kW beam, the overall significance to the mass hierarchy is higher ($\sim 12\sigma$) and the order of decoherence curves corresponding to different values of n obeys a similar trend to that in 90 kW beam. However, since the *MH* sensitivity of P2O (for both 90 and 450 kW) is very high, one can note that the effect of decoherence is not prominent on the determination of *MH*. The same conclusions have been observed in the plots where true hierarchy is assumed to be Inverted Hierarchy (IH).

In the rightmost plots in Figs. 3 and 4, we observe that there is nonzero significance corresponding to *CP*-conserving values of $\delta_{CP} = 0, \pm\pi$ for all values of n. This indicates that the new physics phenomenon of decoherence could induce an extrinsic (fake) *CP* phase and mislead the discovery of the *CP* violation at P2O.

B. Case II (solar limit I): $\Gamma_{21} = \Gamma_{31}, \Gamma_{32} = 0$

The transition probabilities in this case are shown in Fig. 5. From the left plot, one can see no notable change in the ν_e appearance probability compared to the SM for the chosen set of decoherence parameters, and also no extra

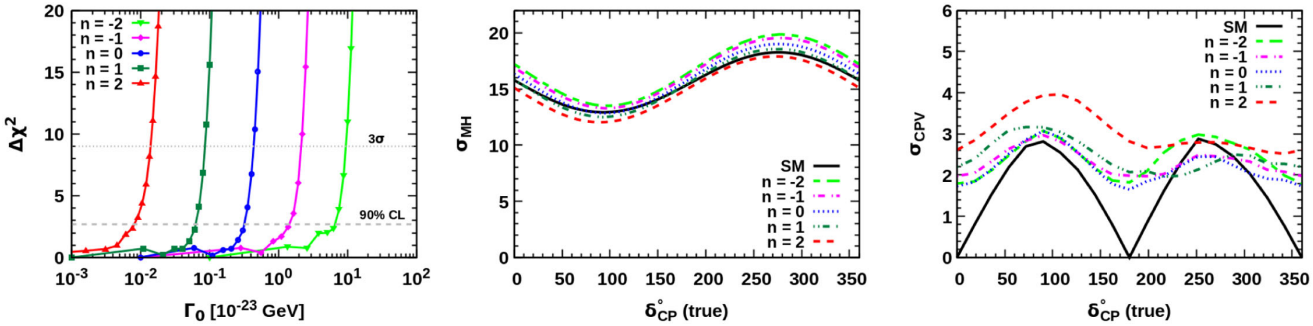

FIG. 4. Case I for P2O-upgrade (450 kW beam power). In the left, we present $\Delta\chi^2$ as a function of Γ_0 (test) based on power-law index $n = 0, \pm 1, \pm 2$. Horizontal dashed and dotted lines stand for 90% and 3σ CL, respectively. In the middle and right panels, we show the significance of the experiment to discover *MH* and *CP* violation.

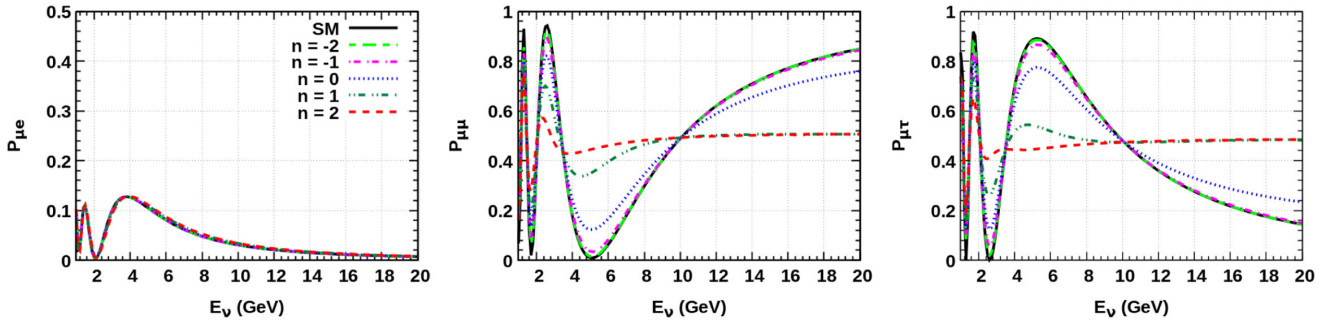

FIG. 5. Probability versus neutrino energy for ν_e appearance (left), ν_μ disappearance (middle), and ν_τ appearance (right) considering case II, $\Gamma_{21} = \Gamma_{31} = 2.3 \times 10^{-23}$ GeV, $\Gamma_{32} = 0$. The different colors correspond to the probabilities for the standard case, and various n dependencies are as mentioned in the legend.

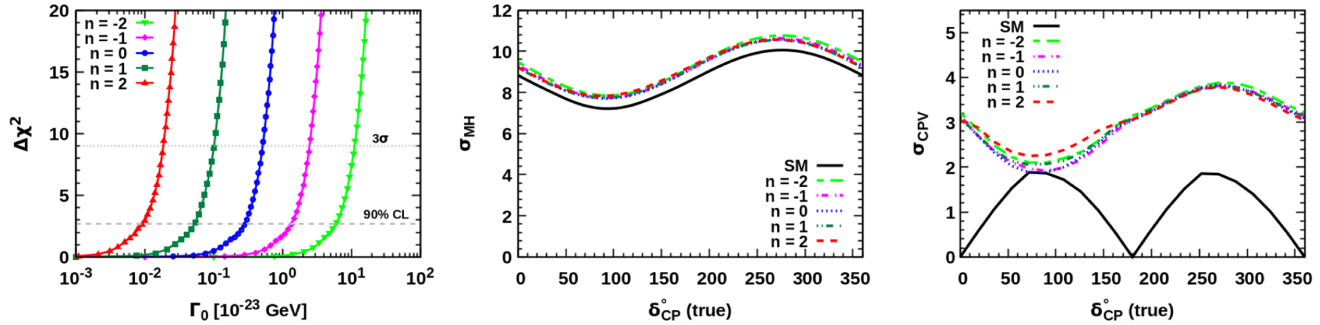

FIG. 6. Case II for the P2O experiment (90 kW beam). In the left, we present $\Delta\chi^2$ as a function of Γ_0 (test) based on power-law index $n = 0, \pm 1, \pm 2$. Horizontal dashed and dotted lines stand for 90% and 3σ CL, respectively. In the middle and right panels, we show the significance of the experiment to discover *MH* and *CP* violation.

peak is observed at $E_\nu \sim 10$ GeV. In the middle plot, the ν_μ disappearance probabilities are presented for different n. Clearly, the probability values significantly vary for the cases with $n \geq 0$. The same can be noted from the rightmost plot showing $\nu_\mu \to \nu_\tau$ probability.

To obtain the bounds on the decoherence parameters, we plot χ^2 vs Γ in the left panel in Figs. 6 and 7. The corresponding bounds of 90% and 3σ CL on Γ are listed in the second column in Tables III and IV. In the middle and the right figures, we present the significance σ_{MH} and σ_{CPV} with respect to true δ_{CP} using 3σ bounds obtained from the left plot. From the middle panel, it is clear that σ_{MH} has not altered significantly for all values of n. However, in the case of σ_{CPV}, we observe that for all true values of δ_{CP} the significance of the P2O experiment is significantly mislead due to the mismatch in the true spectrum and the fit hypothesis.

C. Case III (solar limit II): $\Gamma_{21} = \Gamma_{32}, \Gamma_{31} = 0$

We plot $\nu_\mu \to \nu_e$ transition in the left, $\nu_\mu \to \nu_\mu$ in the middle, and $\nu_\mu \to \nu_\tau$ in the right considering case III in

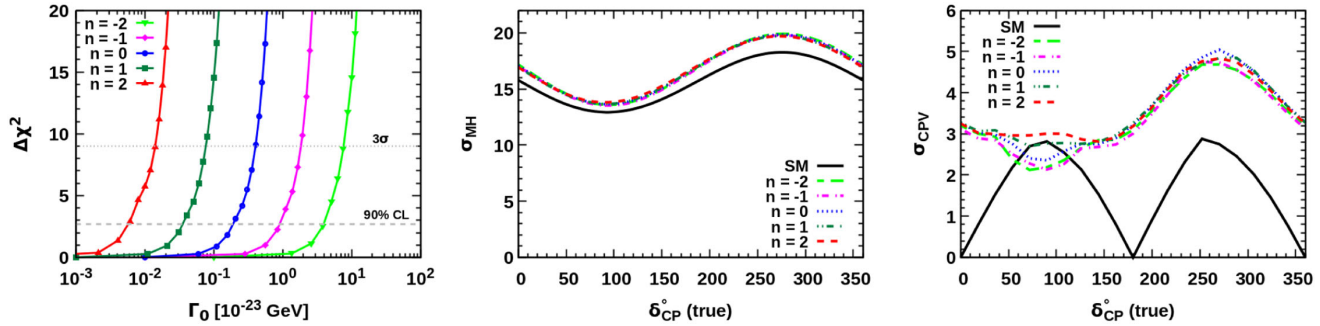

FIG. 7. Case II for P2O-upgrade (450 kW beam power). In the left, we present $\Delta\chi^2$ as a function of Γ_0 (test) based on power-law index $n = 0, \pm 1, \pm 2$. Horizontal dashed and dotted lines stand for 90% and 3σ CL, respectively. In the middle and right panels, we show the significance of the experiment to discover *MH* and *CP* violation.

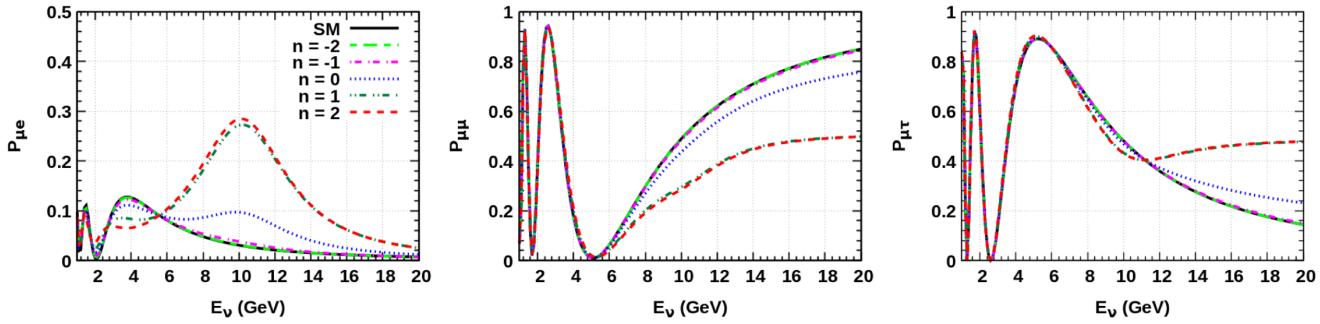

FIG. 8. Probability versus neutrino energy for ν_e appearance (left), ν_μ disappearance (middle), and ν_τ appearance (right) considering case III, $\Gamma_{21} = \Gamma_{32} = 2.3 \times 10^{-23}$ GeV, and $\Gamma_{31} = 0$.

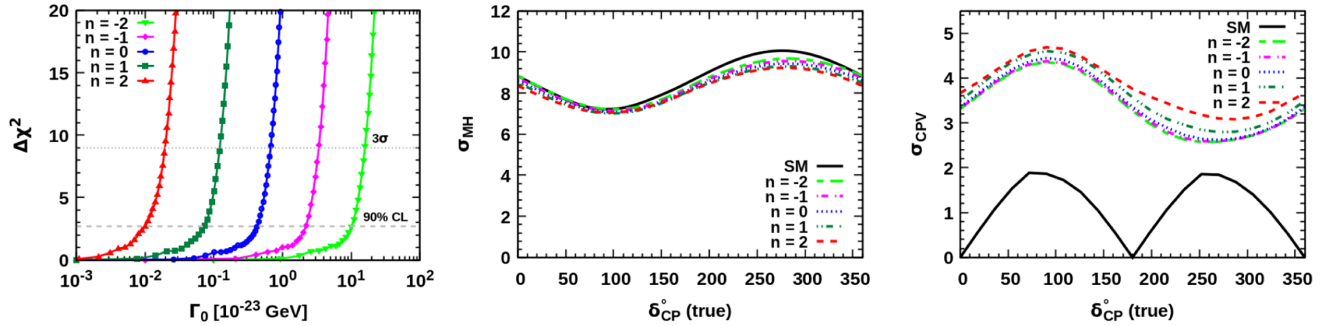

FIG. 9. Case III for the P2O experiment (90 kW beam). In the left, we present $\Delta\chi^2$ as a function of Γ_0 (test) based on power-law index $n = 0, \pm 1, \pm 2$. Horizontal dashed and dotted lines stand for 90% and 3σ CL, respectively. In the middle and right panels, we show the significance of the experiment to discover *MH* and *CP* violation.

Fig. 8. Looking at the left plot, one can state the ν_e appearance probability varies similar to case I. The ν_μ disappearance probability decreases for $E_\nu \geq 6$ GeV, and ν_τ appearance probability increases for $E_\nu \geq 11$ GeV.

The bounds on the decoherence parameters in this case are shown in the left plots in Figs. 9 and 10 and are tabulated in the third column in Tables III and IV. In the middle panel, we plot the *MH* sensitivities, where we can see the σ for all n are lesser than the values corresponding to the SM and the maximum ($\sim 20\sigma$) is visible around 270°. However, in the case of σ_{CPV} for P2O and P2O-upgrade, the discovery potential to *CP* violation is wronged due to the presence of decoherence.

D. Case IV (atmospheric limit): $\Gamma_{31} = \Gamma_{32}, \Gamma_{21} = 0$

We present the oscillation probabilities in Fig. 11 with Γ_{31} and Γ_{32} nonzero and equal. The $P_{\mu e}$ in the left plot is similar to the corresponding plot of cases I and III, but $P_{\mu\mu}$ (in the middle) and $P_{\mu\tau}$ (in the right) differ. $P_{\mu\mu}$ ($P_{\mu\tau}$) increases (decreases) significantly with respect to SM for $n \geq 0$ in the energy range 4–9 GeV.

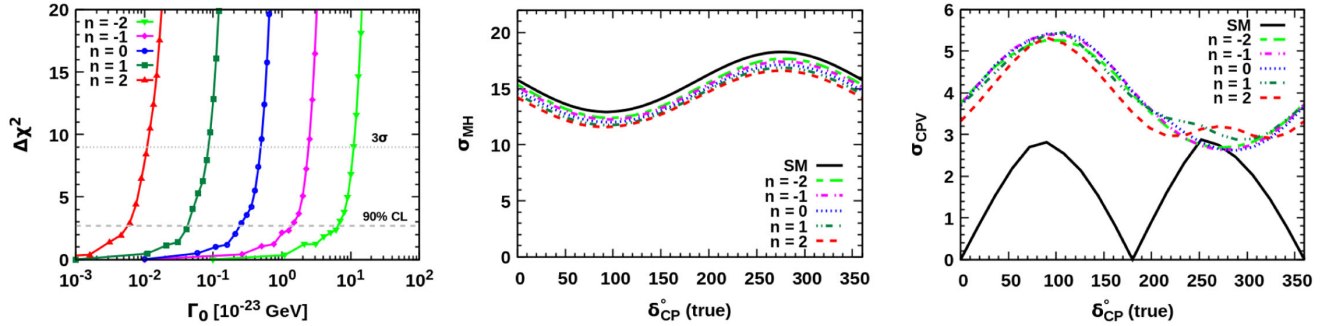

FIG. 10. Case III for P2O-upgrade (450 kW beam power). In the left, we present $\Delta\chi^2$ as a function of Γ_0 (test) based on power-law index $n = 0, \pm 1, \pm 2$. Horizontal dashed and dotted lines stand for 90% and 3σ CL, respectively. In the middle and right panels, we show the significance of the experiment to discover *MH* and *CP* violation.

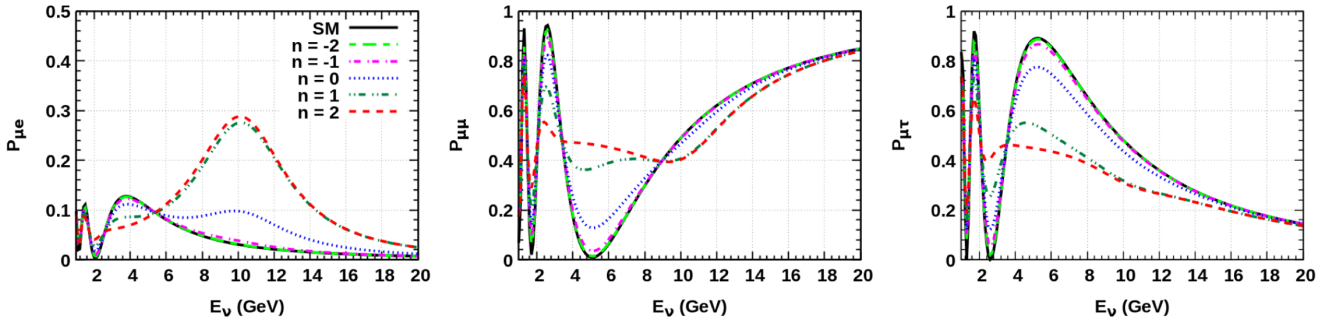

FIG. 11. Probability versus neutrino energy for ν_e appearance (left), ν_μ disappearance (middle), and ν_τ appearance (right) considering case IV, $\Gamma_{31} = \Gamma_{32} = 2.3 \times 10^{-23}$ GeV, and $\Gamma_{21} = 0$.

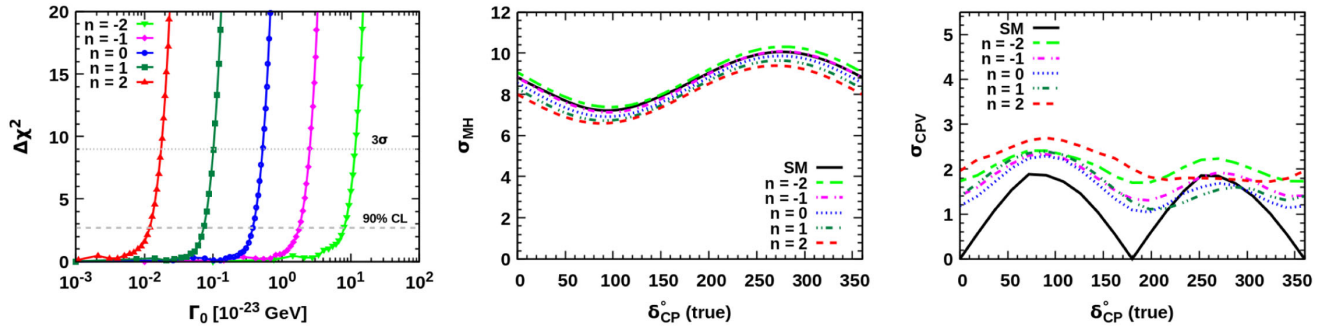

FIG. 12. Case IV for the P2O experiment (90 kW beam). In the left, we present $\Delta\chi^2$ as a function of Γ_0 (test) based on power-law index $n = 0, \pm 1, \pm 2$. Horizontal dashed and dotted lines stand for 90% and 3σ CL, respectively. In the middle and right panels, we show the significance of the experiment to discover *MH* and *CP* violation.

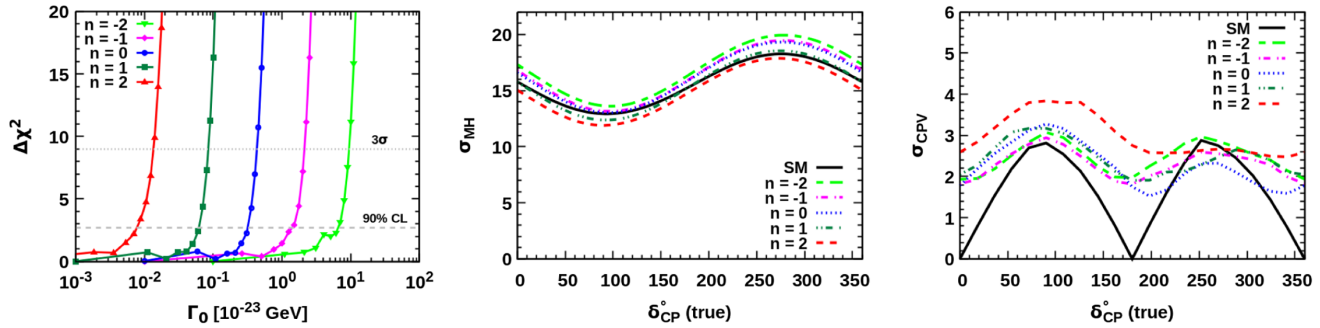

FIG. 13. Case IV for P2O-upgrade (450 kW beam power). In the left, we present $\Delta\chi^2$ as a function of Γ_0 (test) based on power-law index $n = 0, \pm 1, \pm 2$. Horizontal dashed and dotted lines stand for 90% and 3σ CL, respectively. In the middle and right panels, we show the significance of the experiment to discover *MH* and *CP* violation.

Beyond that, both the $P_{\mu\mu}$ and $P_{\mu\tau}$ are lesser than the corresponding SM probability.

Based on the assumption in case IV, in Figs. 12 and 13, we have shown the bounds on Γ in the left panel and the σ_{MH} and the σ_{CPV} in the middle and the right panels, respectively. These plots are similar to the plots in case I, and, hence, the same inferences can be deduced for this case.

E. Discussion

From Figs. 2, 5, 8, and 11, we observe that varying values of n result in distinct spectral distortions of oscillation probabilities in all the scenarios. It is evident from these figures that in all the cases the neutrino oscillation probabilities are sensitive to positive powers of n. This arises due to the high energy range ($E_\nu \geq E_0$) in Eq. (2.13) of the neutrino beam with respect to reference value ($E_0 = 1$ GeV) considered. This result aligns with conclusions drawn in Ref. [44] for the accelerator data. From cases I, III, and IV, it can be seen that $P_{\mu e}$ has the same spectral distortion for all the values of n. In addition, for $n \geq 0$ there is a peak appearing around 10 GeV for these cases. This can be attributed to the nonzero value of Γ_{32} in

these cases. The same conclusion that Γ_{32} affects only the $P_{\mu e}$ channel can be verified from the left plot in Fig. 5 belonging to case II. On the contrary, Γ_{32} does not play a significant role in the $P_{\mu\mu}$ channel for the neutrino energy 2 GeV $< E_\nu <$ 12 GeV. This can be seen from the middle panels in Figs. 5 and 8, where $\Gamma_{32} = 0$ in the former and $\Gamma_{32} \neq 0$ in the latter.

From Tables III and IV, it can be observed that cases I and IV give rise to similar bounds on the Γ parameter. First, $\Gamma_{21} \neq 0$ does not effect the $P_{\mu e}$ channel as can be seen from the left panel in Figs. 2 and 11. Additionally, from the middle panel in Figs. 2 and 11, it can be seen that the difference in $P_{\mu\mu}$ values dominant after $E_\nu \geq 8$ GeV. However, the P2O flux gradually falls after $E_\nu \sim 7$ GeV, and the analysis window for the χ^2 plots is considered as 2 GeV $< E_\nu <$ 12 GeV. Consequently, the bounds on Γ for these cases (cases I and IV) are similar in both the P2O and P2O-upgrade experiments. For the case of $n = 0$ (third row) in Tables III and IV, one can note that the bounds on Γ from P2O and P2O-upgrade would be better than the bounds reported in Ref. [44]. Specifically, case II poses strong constraints on $\Gamma_{jk} \leq 2.76 \times 10^{-24}$ GeV for P2O and $\Gamma_{jk} \leq 1.89 \times 10^{-24}$ GeV for P2O-upgrade, which are found to be better than the bounds reported by T2K and MINOS joint analysis in Ref. [36] and the upcoming DUNE experiment in Ref. [43] and competitive with the recent bounds obtained from neutrinos detected by IceCube in Refs. [40,41]. For $n = -1, -2$, the bounds on Γ_{jk} are $\mathcal{O}(10^{-23})$ at 90% CL. These bounds are less constrained when compared to the bounds from reactor data in Ref. [44] as expected.

V. CONCLUSIONS

In this work, we have investigated the effect of environmentally induced decoherence on the neutrino oscillations at the upcoming P2O experiment. Considering a three-flavor oscillation framework, we study the viable phenomenological models of decoherence where we assume all the decoherence parameters are nonzero (or two of them are nonzero). In both scenarios, we consider a power-law-based relation between the decoherence parameter Γ and the neutrino energy E_ν. After a thorough review of the oscillation probabilities, we note that Γ_{32} plays a significant role on the ν_e appearance channel. Given that in P2O the neutrino beam energy $E_\nu > E_0$ (reference $E_0 = 1$ GeV), we observe that when $n \geq 0$ the effect decoherence on the oscillation probabilities is prominent.

Assuming that there is no decoherence in the true neutrino spectra, we obtain bounds on the Γ_{jk} parameter for both 90 (P2O) and 450 kW proton beams (P2O-upgrade). For the case of $n = 0$, the bounds obtained on Γ_{jk} in both P2O and P2O-upgrade across all the cases would be better than the bounds reported in Ref. [44]. For case II, we obtain $\Gamma_{jk} \leq 2.76 \times 10^{-24}$ GeV for P2O and $\Gamma_{jk} \leq 1.89 \times 10^{-24}$ GeV for P2O-upgrade, which are found to be the most stringent bounds among the bounds reported from other experiments.

Furthermore, we also explore how the discovery potential of P2O and P2O-upgrade is affected if one assumes nonzero decoherence in the true spectrum and standard three-flavor oscillations in the test spectrum. We note that the comprehensive effect of $P_{\mu e}$, $P_{\mu\mu}$, and the corresponding antineutrino probabilities has not significantly affected the *MH* sensitivity of the experiment. However, when we assume the presence of decoherence in nature, a fake nonzero *CP* phase causes a rejection in the null hypothesis; i.e., $\delta_{CP} = 0$, π in all the decoherence models. In conclusion, based on our analysis, it is evident that the P2O experiment shows significant promise in constraining the environmental decoherence parameters.

ACKNOWLEDGMENTS

We thank Anatoly Sokolov for fruitful discussions. We acknowledge Dmitry Zaborov for useful information related to P2O flux. One of the authors (K. N. D.) thanks the Department of Science and Technology (DST)-SERB International Research Experience (SIRE) program for the financial support Grant No. SIR/2022/000518.

[1] S. W. Hawking, Space-time foam, Nucl. Phys. **B144**, 349 (1978).
[2] D. Amati, M. Ciafaloni, and G. Veneziano, Superstring collisions at Planckian energies, Phys. Lett. B **197**, 81 (1987).
[3] S. Das, M. P. G. Robbins, and E. C. Vagenas, Gravitation as a source of decoherence, Int. J. Mod. Phys. D **27**, 1850008 (2017).
[4] T. Stuttard and M. Jensen, Neutrino decoherence from quantum gravitational stochastic perturbations, Phys. Rev. D **102**, 115003 (2020).
[5] L. Petruzziello and F. Illuminati, Quantum gravitational decoherence from fluctuating minimal length and deformation parameter at the Planck scale, Nat. Commun. **12**, 4449 (2021).
[6] Y. Liu, L.-z. Hu, and M.-L. Ge, The effect of quantum mechanics violation on neutrino oscillation, Phys. Rev. D **56**, 6648 (1997).
[7] F.-C. Ma and H.-M. Hu, Testing quantum mechanics in neutrino oscillation, arXiv:hep-ph/9805391.
[8] C.-H. Chang, W.-S. Dai, X.-Q. Li, Y. Liu, F.-C. Ma, and Z.-j. Tao, Possible effects of quantum mechanics violation

induced by certain quantum gravity on neutrino oscillations, Phys. Rev. D **60**, 033006 (1999).
[9] F. Benatti and R. Floreanini, Open system approach to neutrino oscillations, J. High Energy Phys. 02 (2000) 032.
[10] H. V. Klapdor-Kleingrothaus, H. Pas, and U. Sarkar, Effects of quantum space-time foam in the neutrino sector, Eur. Phys. J. A **8**, 577 (2000).
[11] A. M. Gago, E. M. Santos, W. J. C. Teves, and R. Zukanovich Funchal, Quantum dissipative effects and neutrinos: Current constraints and future perspectives, Phys. Rev. D **63**, 073001 (2001).
[12] F. Benatti and R. Floreanini, Massless neutrino oscillations, Phys. Rev. D **64**, 085015 (2001).
[13] G. L. Fogli, E. Lisi, A. Marrone, and D. Montanino, Status of atmospheric $\nu_\mu \to \nu_\tau$ oscillations and decoherence after the first K2K spectral data, Phys. Rev. D **67**, 093006 (2003).
[14] Y. Ashie *et al.*, Evidence for an oscillatory signature in atmospheric neutrino oscillation, Phys. Rev. Lett. **93**, 101801 (2004).
[15] L. A. Anchordoqui, H. Goldberg, M. C. Gonzalez-Garcia, F. Halzen, D. Hooper, S. Sarkar, and T. J. Weiler, Probing Planck scale physics with IceCube, Phys. Rev. D **72**, 065019 (2005).
[16] G. Barenboim, N. E. Mavromatos, S. Sarkar, and A. Waldron-Lauda, Quantum decoherence and neutrino data, Nucl. Phys. **B758**, 90 (2006).
[17] Y. Farzan, T. Schwetz, and A. Y. Smirnov, Reconciling results of LSND, MiniBooNE and other experiments with soft decoherence, J. High Energy Phys. 07 (2008) 067.
[18] R. L. N. Oliveira and M. M. Guzzo, Quantum dissipation in vacuum neutrino oscillation, Eur. Phys. J. C **69**, 493 (2010).
[19] R. L. N. Oliveira and M. M. Guzzo, Dissipation and θ_{13} in neutrino oscillations, Eur. Phys. J. C **73**, 2434 (2013).
[20] R. L. N. Oliveira, Dissipative effect in long baseline neutrino experiments, Eur. Phys. J. C **76**, 417 (2016).
[21] J. A. B. Coelho and W. A. Mann, Decoherence, matter effect, and neutrino hierarchy signature in long baseline experiments, Phys. Rev. D **96**, 093009 (2017).
[22] J. Carpio, E. Massoni, and A. M. Gago, Revisiting quantum decoherence for neutrino oscillations in matter with constant density, Phys. Rev. D **97**, 115017 (2018).
[23] J. C. Carrasco, F. N. Díaz, and A. M. Gago, Probing CPT breaking induced by quantum decoherence at DUNE, Phys. Rev. D **99**, 075022 (2019).
[24] L. Buoninfante, A. Capolupo, S. M. Giampaolo, and G. Lambiase, Revealing neutrino nature and CPT violation with decoherence effects, Eur. Phys. J. C **80**, 1009 (2020).
[25] P. C. de Holanda, Solar neutrino limits on decoherence, J. Cosmol. Astropart. Phys. 03 (2020) 012.
[26] J. Wang *et al.*, Damping signatures at JUNO, a medium-baseline reactor neutrino oscillation experiment, J. High Energy Phys. 06 (2022) 062.
[27] T. Cheng, M. Lindner, and W. Rodejohann, Microscopic and macroscopic effects in the decoherence of neutrino oscillations, J. High Energy Phys. 08 (2022) 111.
[28] J. C. Carrasco-Martínez, F. N. Díaz, and A. M. Gago, Uncovering the Majorana nature through a precision measurement of the CP phase, Phys. Rev. D **105**, 035010 (2022).
[29] C. Giunti and C. W. Kim, Coherence of neutrino oscillations in the wave packet approach, Phys. Rev. D **58**, 017301 (1998).
[30] M. Blennow, T. Ohlsson, and W. Winter, Damping signatures in future neutrino oscillation experiments, J. High Energy Phys. 06 (2005) 049.
[31] E. Akhmedov, D. Hernandez, and A. Smirnov, Neutrino production coherence and oscillation experiments, J. High Energy Phys. 04 (2012) 052.
[32] Y.-L. Chan, M. C. Chu, K. M. Tsui, C. F. Wong, and J. Xu, Wave-packet treatment of reactor neutrino oscillation experiments and its implications on determining the neutrino mass hierarchy, Eur. Phys. J. C **76**, 310 (2016).
[33] A. de Gouvêa, V. De Romeri, and C. A. Ternes, Combined analysis of neutrino decoherence at reactor experiments, J. High Energy Phys. 06 (2021) 042.
[34] E. Lisi, A. Marrone, and D. Montanino, Probing possible decoherence effects in atmospheric neutrino oscillations, Phys. Rev. Lett. **85**, 1166 (2000).
[35] R. L. N. de Oliveira, M. M. Guzzo, and P. C. de Holanda, Quantum dissipation and CP violation in MINOS, Phys. Rev. D **89**, 053002 (2014).
[36] A. L. G. Gomes, R. A. Gomes, and O. L. G. Peres, Quantum decoherence and relaxation in long-baseline neutrino data, J. High Energy Phys. 10 (2023) 035.
[37] G. L. Fogli, E. Lisi, A. Marrone, D. Montanino, and A. Palazzo, Probing non-standard decoherence effects with solar and KamLAND neutrinos, Phys. Rev. D **76**, 033006 (2007).
[38] G. Balieiro Gomes, M. M. Guzzo, P. C. de Holanda, and R. L. N. Oliveira, Parameter limits for neutrino oscillation with decoherence in KamLAND, Phys. Rev. D **95**, 113005 (2017).
[39] J. A. B. Coelho, W. A. Mann, and S. S. Bashar, Nonmaximal θ_{23} mixing at NOvA from neutrino decoherence, Phys. Rev. Lett. **118**, 221801 (2017).
[40] P. Coloma, J. Lopez-Pavon, I. Martinez-Soler, and H. Nunokawa, Decoherence in neutrino propagation through matter, and bounds from IceCube/DeepCore, Eur. Phys. J. C **78**, 614 (2018).
[41] R. Abbasi *et al.*, Searching for decoherence from quantum gravity at the IceCube South Pole Neutrino Observatory, Nat. Phys. **20**, 913 (2024).
[42] J. A. Carpio, E. Massoni, and A. M. Gago, Testing quantum decoherence at DUNE, Phys. Rev. D **100**, 015035 (2019).
[43] G. Balieiro Gomes, D. V. Forero, M. M. Guzzo, P. C. De Holanda, and R. L. N. Oliveira, Quantum decoherence effects in neutrino oscillations at DUNE, Phys. Rev. D **100**, 055023 (2019).
[44] V. De Romeri, C. Giunti, T. Stuttard, and C. A. Ternes, Neutrino oscillation bounds on quantum decoherence, J. High Energy Phys. 09 (2023) 097.
[45] J. Aguilar *et al.*, Decoherence in neutrino oscillation at the ESSnuSB experiment, arXiv:2404.17559.
[46] A. V. Akindinov *et al.*, Letter of interest for a neutrino beam from protvino to KM3NeT/ORCA, Eur. Phys. J. C **79**, 758 (2019).
[47] S. Adrian-Martinez *et al.*, Letter of intent for KM3NeT 2.0, J. Phys. G **43**, 084001 (2016).

[48] G. Lindblad, On the generators of quantum dynamical semigroups, Commun. Math. Phys. **48**, 119 (1976).
[49] V. Gorini, A. Kossakowski, and E. C. G. Sudarshan, Completely positive dynamical semigroups of N level systems, J. Math. Phys. (N.Y.) **17**, 821 (1976).
[50] V. Gorini, A. Frigerio, M. Verri, A. Kossakowski, and E. C. G. Sudarshan, Properties of quantum Markovian master equations, Rep. Math. Phys. **13**, 149 (1978).
[51] T. Banks, L. Susskind, and M. E. Peskin, Difficulties for the evolution of pure states into mixed states, Nucl. Phys. **B244**, 125 (1984).
[52] F. Benatti and H. Narnhofer, Entropy behavior under completely positive maps, Lett. Math. Phys. **15**, 325 (1988).
[53] P. B. Denton and S. J. Parke, Addendum to Compact perturbative expressions for neutrino oscillations in matter J. High Energy Phys. 06 (2018) 109.
[54] P. Huber, M. Lindner, and W. Winter, Simulation of long-baseline neutrino oscillation experiments with GLoBES (General Long Baseline Experiment Simulator), Comput. Phys. Commun. **167**, 195 (2005).
[55] P. Huber, J. Kopp, M. Lindner, M. Rolinec, and W. Winter, New features in the simulation of neutrino oscillation experiments with GLoBES 3.0: General long baseline experiment simulator, Comput. Phys. Commun. **177**, 432 (2007).
[56] G. L. Fogli, E. Lisi, A. Marrone, D. Montanino, and A. Palazzo, Getting the most from the statistical analysis of solar neutrino oscillations, Phys. Rev. D **66**, 053010 (2002).
[57] P. Huber, M. Lindner, and W. Winter, Superbeams versus neutrino factories, Nucl. Phys. **B645**, 3 (2002).
[58] I. Esteban, M. C. Gonzalez-Garcia, M. Maltoni, T. Schwetz, and A. Zhou, The fate of hints: Updated global analysis of three-flavor neutrino oscillations, J. High Energy Phys. 09 (2020) 178.